Mechanism of Interaction between the General Anesthetic Halothane and a Model Ion Channel Protein, II: Fluorescence and Vibrational Spectroscopy Using a Cyanophenylalanine Probe

Jing Liu,[†] Joseph Strzalka,[†] Andrey Tronin,[†] Jonas S. Johansson,[‡] and J. Kent Blasie[†*]
[†]Departments of Chemistry and [‡]Anesthesiology and Critical Care, University of Pennsylvania, Philadelphia, Pennsylvania

ABSTRACT We demonstrate that cyano-phenylalanine (Phe_{CN}) can be utilized to probe the binding of the inhalational anesthetic halothane to an anesthetic-binding, model ion channel protein hbAP-Phe_{CN}. The Trp to Phe_{CN} mutation alters neither the α-helical conformation nor the 4-helix bundle structure. The halothane binding properties of this Phe_{CN} mutant hbAP-Phe_{CN}, based on fluorescence quenching, are consistent with those of the prototype, hbAP1. The dependence of fluorescence lifetime as a function of halothane concentration implies that the diffusion of halothane in the nonpolar core of the protein bundle is one-dimensional. As a consequence, at low halothane concentrations, the quenching of the fluorescence is dynamic, whereas at high concentrations the quenching becomes static. The 4-helix bundle structure present in aqueous detergent solution and at the air-water interface, is preserved in multilayer films of hbAP-Phe_{CN}, enabling vibrational spectroscopy of both the protein and its nitrile label (-CN). The nitrile groups' stretching vibration band shifts to higher frequency in the presence of halothane, and this blue-shift is largely reversible. Due to the complexity of this amphiphilic 4-helix bundle model membrane protein, where four Phe_{CN} probes are present adjacent to the designed cavity forming the binding site within each bundle, all contributing to the infrared absorption, molecular dynamics (MD) simulation is required to interpret the infrared results. The MD simulations indicate that the blue-shift of -CN stretching vibration induced by halothane arises from an indirect effect, namely an induced change in the electrostatic protein environment averaged over the four probe oscillators, rather than a direct interaction with the oscillators. hbAP-Phe_{CN} therefore provides a successful template for extending these investigations of the interactions of halothane with the model membrane protein via vibrational spectroscopy, using cyano-alanine residues to form the anesthetic binding cavity.

INTRODUCTION

The mechanism of inhalational anesthetic action has been studied for decades but remains unclear. One of the more recent theories of inhalational anesthetic action is that anesthetic compounds preferentially bind to membrane proteins, ligand-gated ion channels in particular, which play a key role in neurological signal transmission in the central and peripheral nervous systems. The anesthetics are suggested to associate with cavities, which exist ubiquitously in these membrane proteins, thereby lowering the free energy and stabilizing the system (1,2). However, these natural membrane proteins are large and complex generally comprised of multiple subunits (or domains), making them difficult to study directly by sophisticated chemical or physical techniques. The weak binding of these compounds to proteins thought to be of physiological relevance to anesthetic action further contributes significantly to this difficulty. Therefore, a variety of simplified model proteins have been designed more recently for this purpose as studied over the past 10 years.

Among the model proteins designed to mimic the anesthetic's target, the halothane-binding, amphiphilic 4-helix bundle proteins are most closely related to the natural membrane proteins (3,4). This type of model membrane protein has been designed to possess a hydrophobic domain based on a synthetic ion channel and a hydrophilic domain with a designed cavity within its nonpolar core. Halothane binds to the cavity with an affinity close to the physiologically relevant range. Because the amphiphilic halothane binding protein can be vectorially oriented at the air-water interface, it can be subsequently transferred onto solid supports via Langmuir-Blodgett (LB) or Langmuir-Schaeffer deposition with the binding properties preserved (5). In the above studies, steady-state fluorescence spectroscopy of an adjacent aromatic residue, e.g., Trp, has been the major spectroscopic technique to study the association of halothane with the designed cavity. However, fluorescence quenching can result from either a dynamic collisional interaction between the anesthetic molecule and the fluorophore or a static interaction arising from complex formation. As a result of the former, this phenomenon can always be observed even when such a designed binding cavity does not exist, although the quenching efficiency is diminished (3,6).

Infrared spectroscopy has been widely used to monitor both protein structure and dynamics. This technique is sufficiently sensitive to detect changes in protein conformation as well as changes in the local environment of an individual amino-acid side chain (7). With infrared spectroscopy, we might directly determine the anesthetic molecule's target by isotopically labeling the putative binding site and monitoring the changes induced by the anesthetic ligand. Alternatively, we can label the potential binding site with a small infrared-active functional group, such as the nitrile group -CN, and place

Submitted August 13, 2008, and accepted for publication January 7, 2009.

*Correspondence: jkblasie@sas.upenn.edu

Editor: Thomas J. McIntosh.

© 2009 by the Biophysical Society

0006-3495/09/05/4176/12 $2.00

doi: 10.1016/j.bpj.2009.01.055

such a probe on the side chain of a residue at or near the binding site. For example, Yoshikawa et al. (8) uses the -CN vibrational stretching band as a marker to investigate ligand binding in hemeproteins. Recently, Getahun et al. (9), Tucker et al. (10), and Mukherjee et al. (11) has shown that the nitrile-labeled amino acids can be used as local environment reporters in model proteins.

The nitrile group has become a popular vibrational probe because this group is small and well accommodated in both polar and nonpolar environments. The -CN stretching band is centered ~2250 cm^{-1} (12). This spectral region is transparent for most proteins making the band assignment straightforward when using this probe in a new system. In addition to serving as a vibrational infrared probe, the -CN-labeled Phe was also discovered to have a fluorescence quantum yield somewhat larger than Trp (13), unlike Phe itself. Thus, as the first step in applying infrared spectroscopy to study halothane binding to oriented samples of amphiphilic model membrane protein, we decided to choose Phe_{CN} as the probe adjacent to the halothane binding cavity with the advantage that the protein-anesthetic interaction can be investigated via both fluorescence and infrared spectroscopic techniques simultaneously.

In this work, we demonstrate the applicability of the Phe_{CN} probe for studying the binding of halothane to the model membrane ion channel protein hbAP-Phe_{CN}. The protein sequence was based on the Trp-labeled halothane binding amphiphilic protein (hbAP1) (4), with the sole mutation of $W15F_{CN}$. This protein was investigated in three forms with various techniques. Because of the low protein solubility in detergent solution and the limited sensitivity of the instrument, the Fourier transform infrared spectroscopy measurements were necessarily performed on LB multilayer films of the protein. Because a Langmuir monolayer film is the precursor to LB multilayer films, x-ray reflectivity and grazing-incidence x-ray diffraction (GIXD) measurements were carried out on the Langmuir monolayer to validate that the α-helical conformation and 4-helix bundle structure are not influenced by the mutation. Circular dichroism (CD) spectroscopy, steady-state fluorescence quenching, and fluorescence lifetime analysis were also performed with hbAP-Phe_{CN} in isotropic detergent solution to evaluate the helical content, halothane binding affinity, and the fluorescence quenching mechanism upon halothane incorporation into the protein bundle. By comparing these results with those for the parent hbAP1 investigated under analogous conditions, it can be concluded that the mutation does not affect the α-helical content, 4-helix bundle formation, or the halothane binding affinity. Subsequent to the above investigations, the protein was transferred onto solid germanium (Ge) or quartz substrates in the form of multilayer films by LB-deposition. These specimens, providing sufficient protein density for the infrared measurements, were characterized by x-ray reflectivity to determine the thickness of the films, by steady-state fluorescence spectroscopy to evaluate the halothane binding affinity in the films, and by attenuated total reflection Fourier transform infrared (ATR-FTIR) spectroscopy to investigate the orientation of the helices with respect to the substrate surface and the effect of halothane on the nitrile stretching vibrational band. The -CN stretching vibration was found to exhibit a reversible blue-shift upon the addition of halothane up to concentrations sufficient to quench Phe_{CN} fluorescence. With the assistance from MD simulations, the experimentally observed blue-shift is attributed to an indirect effect of halothane, namely induced changes in the local electrostatic protein environment surrounding the -CN probe oscillators.

MATERIALS AND METHODS

Materials

9-Fluorenylmethoxycarbonyl (Fmoc)-protected L-α-amino acids and Fmoc-amide resin were purchased from Applied Biosystems (Foster City, CA). Halothane (2-bromo-2-chloro-1,1,1-trifluoroethane) was obtained from Sigma (St. Louis, MO). The thymol preservative in the commercial halothane was removed with an aluminum oxide column (14). The detergent *N*-octyl-β-*D*-glucopyranoside (OG) was from Anatrace (Maumee, OH). All other solvents and reagents were purchased from either Fisher Scientific (Springfield, NJ) or Sigma (St. Louis, MO).

Protein synthesis and purification

The protein hbAP-Phe_{CN} was assembled as C-terminus carboxyamide on an Applied Biosystems Model 433A (Applied Biosystems, Foster City, CA) solid-phase protein synthesizer using the standard Fmoc/tBu protection strategy on an Fmoc-amide resin at 0.25-mmol scale. The crude protein was protected by acetylation at its N-terminus in 1:1 (v/v) acetic anhydride-pyridine (stirring for 30 min) and purified on a reversed-phase C4 HPLC column (Vydac, Columbia, MD) using gradients of 6:3:1 isopropanol/acetonitrile/H_2O and water containing 0.1% (v/v) 2,2,2-trifluoroacetic acid. The protein's identity was verified by matrix-assisted laser desorption/ionization mass spectrometry. Pure protein (4.63 kDa molecular mass) was dimerized by oxidizing its C-terminal Cys in 1:1 (v/v) 100 mM ammonium hydrogen carbonate buffer (pH 10.0), and isopropanol in air to form the 80-amino-acid protein dimer linked by a disulfide bond (9.26 kDa molecular mass).

Specimen preparation

hbAP-Phe_{CN} was later investigated in three forms, namely in isotropic detergent solution, in Langmuir monolayers at the air-water interface and in LB multilayer films on solid substrates. The molar extinction coefficient for hbAP-Phe_{CN} was determined experimentally to be $12{,}000 \pm 200\ M^{-1}\ cm^{-1}$ at 240 nm, using Beer's Law, because the ultraviolet (UV) absorption maximum for hbAP-Phe_{CN} is shifted slightly to longer wavelength, compared to that reported for Phe_{CN} itself, with a molar extinction of $13{,}000 \pm 500\ M^{-1}\ cm^{-1}$ at 233 nm (13). The concentrations of all protein solutions utilized in this work were determined spectrophotometrically using this value.

Aqueous detergent solutions

UV-visible spectroscopy, CD, and steady-state fluorescence measurements were carried out in buffer solutions containing 0.9% OG, 50 mM potassium phosphate (KPi), and 500 mM potassium chloride (KCl) at pH 7.0.

Langmuir monolayers at the air-water interface

Characterization at the air-water interface, including surface pressure (π)-area (A) isotherms, x-ray reflectivity, and GIXD, were preformed on

Langmuir monolayers. These were prepared by spreading hbAP-Phe_{CN} in methanol onto the meniscus of a glass capillary at an oblique angle passing through the air-water interface. The aqueous subphase contained 1 mM KPi and 10 mM KCl at pH 8.0. At least 10 min was allowed for methanol evaporation before compressing the monolayer at a rate of ~20 $Å^2$/helix/min.

LB multilayer films on solid supports

LB multilayer films were formed via monolayer-by-monolayer deposition onto quartz slides (fused silica, UV grade; 25 × 35 mm^2, from Esco Products, NJ) for x-ray reflectivity and fluorescence measurements or onto Ge internal reflection elements (Ge-IRE) (50 × 10 × 2 mm^3 SPT 45°, from Harrick Scientific, Pleasantville, NY) for infrared studies. Both quartz and Ge-IRE substrates were cleaned and then alkylated with octadecyltrichlorosilane (OTS) producing a methyl-terminated nonpolar surface. The detailed procedure of cleaning and alkylating substrates and subsequent LB-deposition are described in an earlier study (5). In brief, the quartz or Ge-IRE substrates were first cleaned by sonicating for 10 min consecutively in detergent solution, methanol, chloroform, and acetone and then subjected to plasma cleaning for ~15 min (Harrick Scientific, Pleasantville, NY). Alkylation with OTS was done by sonicating the substrates for 20 min in a solution with 0.1% OTS in 80% hexadecane, 12% carbon tetrachloride, and 8% chloroform (by volume). One quartz slide and one Ge-IRE slide were clamped side by side at the end of a rigid rod connected to a motorized translation stage. The underside of the Ge-IRE slide was covered with rubber to prevent film deposition. The slides were then simultaneously passed vertically downward through the hbAP-Phe_{CN} monolayer, which was compressed to and maintained at 35 mN/m on an aqueous subphase of 1 mM KPi and 10 mM KCl at pH 6.7. The speed was maintained constant at 3 mm/min until the slides were fully submerged in the subphase. They were then withdrawn upward at the same speed through the monolayer. This cyclic process was repeated five times at 22°C to fabricate the multilayer films. These films were anticipated to consist of a maximum of five monolayers of hbAP-Phe_{CN}, with apposed hydrophilic-to-hydrophobic domains across neighboring layers due to the *Z*-type deposition observed, namely with deposition only during the upstroke.

Isotherms and x-ray characterization of Langmuir monolayers

Surface pressure-area isotherms were collected on a commercial Langmuir trough (Lauda, Lauda-Königshofen, Germany) for Langmuir monolayers of hbAP-Phe_{CN} using the method described by Ye et al. (3).

X-ray reflectivity data were recorded on beamline X-22B at the National Synchrotron Light Source at Brookhaven National Laboratory (Upton, NY). Data for hbAP-Phe_{CN} monolayers at the air-water interface were collected at constant surface pressures or constant areas (for $\pi > 30$ mN/m). At higher surface pressures, we relied on the area/α-helix instead of surface pressure because the Wilhelmy-plate utilized for the latter did not penetrate through the monolayer vertically, typical of more solid-like monolayers. GIXD data were collected on sector 9 at the Advanced Photon Source, Argonne National Laboratory (Argonne, IL). The setups and procedures for these two different x-ray scattering experiments were described thoroughly elsewhere (3,5), as well as the related data collection, reduction, and analysis. The only difference here was the background correction in GIXD data reduction. Instead of choosing the scattering from the aqueous subphase alone as the background, GIXD data from a monolayer of 1,2-dilignoceroyl-*sn*-glycero-3-phosphocholine, recorded under identical experimental conditions, were subtracted from the two-dimensional data to eliminate background scattering effects before integration to provide both the q_{xy}- and q_z-dependence of GIXD data from the hbAP-Phe_{CN} monolayer.

CD spectroscopy

The far UV CD spectra were measured for hbAP-Phe_{CN} in detergent solution with a 62A DS spectropolarimeter (Aviv, Lakewood, NJ) utilizing a 1 mm rectangular cuvette at 25°C. Spectra were recorded over the range from 200 to 260 nm with a time constant of 4 s at a 1 nm spectral resolution. The protein concentration was 30–40 μM. The percentage of α-helical content, f_H, was estimated by measuring the mean residue ellipticity at 222 nm, θ_{222}, using the following equation:

$$f_H = (\theta_{222} - \theta_c)/(\theta_H - \theta_c), \quad (1)$$

where θ_c and θ_H are limiting values of θ_{222} for a complete random coil and an infinite helix, respectively. The value of θ_c was assumed to be −3400 deg*cm^2/dmol (15), and θ_H was calculated using the following equation (16):

$$\theta_H = (250T - 44000)(1 - 3/n), \quad (2)$$

where T is the temperature in Celsius and n is the number of residues.

Steady-state fluorescence measurements

The binding affinity of hbAP-Phe_{CN} was determined by steady-state intrinsic Phe_{CN} fluorescence measurements using a RF-5301PC-spectrofluorophotometer (Shimadzu, Kyoto, Japan). The solution sample was contained in a 10 mm square quartz cell with a Teflon stopper and the LB multilayer specimen was held with a homemade slide holder fitting within the cell so that the plane of the slide was along the cell diagonal. Phe_{CN} was excited at 240 nm (bandwidth 3 nm), and emission spectra (bandwidth 5 nm) were recorded at 90° with respect to the incident excitation exhibiting a maximum at 293 nm. The procedure of halothane titration was the same as described in previous studies (3,5). The maximum quenching at an infinite halothane concentration (Q_{max}) and the dissociation constant (K_d) for halothane binding in the vicinity of the Phe_{CN} residues were determined by fitting the data to the following equation (6):

$$\frac{F}{F_0} = 1 - Q_{max}[\text{Halothane}]/(K_d + [\text{Halothane}]), \quad (3)$$

where F_0 and F are the fluorescence in the absence and presence of halothane, respectively. The data reported are the averages of three measurements and presented in the form of mean ± SD.

Fluorescence lifetime acquisition and analysis

Fluorescence excited state lifetime data were obtained using the instrument at the Regional Laser and Biomedical Technology Laboratories at the University of Pennsylvania (Philadelphia, PA). A detailed description on the instrument is provided elsewhere (17). hbAP-Phe_{CN} in aqueous detergent solution with varying halothane concentrations was studied in a gas-tight quartz cell with 10 mm path length. The protein concentration was 70 μM. Fluorescence was excited with a laser pulse centered at 275 nm, and the emission decays were collected at 315 nm with a bandwidth of 10 nm. Steady-state fluorescence spectra were recorded before and after each lifetime acquisition to double check the quenching status. Lifetimes were calculated by fitting the fluorescence decay with multiexponentials: $I(t) = \int_{-\infty}^{t} IRF(t') \sum_{i=1}^{n} A_i e^{-\frac{t-t'}{\tau_i}} dt'$, where *IRF* is the instrument response function, τ_i and A_i are the lifetime and the preexponential factor of *i*th component, respectively. Curve fitting was performed with FluoFit (PicoQuant, Berlin, Germany) software. Global chi-squared minimization and a random distribution of residuals were utilized as goodness-of-fit criteria. The data presented are from experiments performed on two hbAP-Phe_{CN} solution specimens prepared independently.

X-ray reflectivity from LB multilayer films on alkylated quartz

X-ray reflectivity from LB multilayer films was collected using a triple-axis diffractometer with an Enraf-Nonius F-591 rotating-anode x-ray source and

a scintillation detector. A curved LiF crystal was utilized to select and collimate the CuKα_1 spectral line. Further collimation was achieved by the slits before and after the sample chamber, with the resolution determined by the analyzer crystal before the scintillation detector. Reflectivity data were recorded over the range of photon momentum transfer q_z of 0.01 – 0.3 Å^{-1}, defining$q_z = (4\pi/\lambda)\sin\theta$. At lower incident angles, the x-ray beam was attenuated by nickel foils inserted upstream from the specimen. The specimen chamber with Kapton windows was maintained at 4°C. A LI-610 dewpoint generator (LI-COR, Lincoln, NE) was additionally fitted to maintain the relative humidity of the multilayer film's environment in the chamber in excess of 90% in helium.

Infrared spectroscopy of multilayer films on alkylated germanium

Infrared spectra were collected for LB multilayer films deposited on Ge-IRE substrates with a Nicolet (Waltham, MA) Magna-Infrared 860 spectrometer with an ATR attachment (Harrick Scientific, Pleasantville, NY). The incidence angle in the Ge-IRE was 45°. The infrared light source was polarized. Both parallel and perpendicular (with respect to the plane of the Ge surface) components of hbAP-Phe$_{CN}$ infrared absorption were collected from 600 to 4000 cm^{-1} under N_2 atmosphere humidified by D_2O. With the intention of investigating the effect from halothane binding and the reversibility of this effect, the sample was subsequently flushed with halothane saturated moist N_2 and subsequently purged with moist N_2 flow. At least 25 min were required after each change in the specimen's environment to reach equilibrium before data collection. Gas delivery was achieved with a homemade gas mixer. Spectra from otherwise identical alkylated Ge substrates lacking only the protein multilayer were recorded for background correction. Both data and background spectra were the averages of 256 scans with a resolution of 2 cm^{-1} at 25°C. Background subtraction and linear baseline correction were applied before further analysis. The average tilt-angle, with respect to the normal to the substrate surface, was evaluated based on the dichroic ratio ($R^{ATR} = A_{//}/A_{\perp}$) of amide I band, using the following equation (18):

$$\beta = \arccos\sqrt{\frac{2S_{helix} + 1}{3}},$$

where S_{helix} is α-helical order parameter, which can be calculated from the experimentally determined order parameter, $S_{experimental}$, and the angle between the vibrational dipole and the helical axis, α, according to the following equation:

$$S_{helix} = \frac{2S_{experimental}}{3\cos^2\alpha - 1}.$$

$S_{experimental}$ is related to the measured dichroic ratio R^{ATR}:

$$R^{ATR} = \frac{I_x}{I_y} + \frac{I_z}{I_y}\left(1 + \frac{3S_{experimental}}{1 - S_{experimental}}\right),$$

where I_x, I_y, and I_z are the intensities of the evanescent field in the thin film at the Ge-IRE/film interface, which were calculated by assuming the refractive index of the protein multilayer is 1.42 (19,20). The angle α was assumed to be 39° (19).

RESULTS AND DISCUSSION

Protein design

The design for hbAP-Phe$_{CN}$ is based on hbAP1, a halothane-binding, amphiphilic 4-helix bundle model membrane protein with one designed cavity and adjacent Trp residues (4). The sequences of hbAP-Phe$_{CN}$ and hbAP1 are provided in Fig. 1. Trp^{15} is mutated to Phe$_{CN}$ because the latter serves as an environmental-sensitive vibrational probe (9) as well as a fluorophore with high quantum yield (13). This allowed us to investigate the interaction of halothane with the protein hbAP-Phe$_{CN}$ with both infrared and fluorescence spectroscopy simultaneously. Phe$_{CN}$ is similar in size to Trp and therefore this substitution was not expected to significantly affect the protein conformation. In addition, Met^{22} and Leu^{25} were exchanged in position to place the Met residue at a heptad e position. This mutation was expected to improve the binding affinity (21).

hbAP-Phe$_{CN}$

a g f e d c b a

Ac – LKKLREE LAKLFEE *F$_{CN}$*KKL**A**EE *LLLMALL* QLLLALL QLGGC – *CONH$_2$*

hbAP1

a g f e d c b a

Ac – LKKLREE LAKLFEE *W*KKL**A**EE *MLLLA*LL QLLLALL QLGGC – *CONH$_2$*

FIGURE 1 Sequence of hbAP-Phe$_{CN}$. The mutated amino acids are represented in italic type. The designed binding site is highlighted in bold. The sequence of hbAP1 is illustrated for comparison.

Langmuir monolayer characterization at the air-water interface

Surface pressure-area isotherm

Characterization of Langmuir monolayers of the model membrane protein at the air-water interface was performed to verify the coiled coil 4-helix bundle conformation of hbAP-Phe$_{CN}$. The amphiphilic character of the bundle is seen to be preserved from the surface pressure-area isotherm. As seen in Fig. 2, the form of the isotherm is similar to that obtained with the parent hbAP1 under analogous conditions, shown in Fig. S4 in the Supporting Material for the

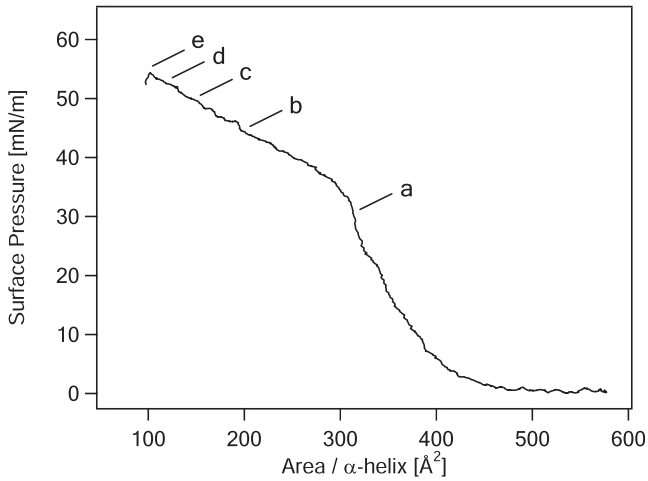

FIGURE 2 Surface pressure-area isotherm of hbAP-Phe$_{CN}$ collected on the subphase of 1 mM KPi and 10 mM KCl at pH 8.0. hbAP-Phe$_{CN}$ was spread from methanol solution. The letters represent the points where x-ray reflectivity data were recorded. *a* indicates the surface pressure of 30 mN/m, and *b*–*e* are the areas of 200, 150, 120, 100 Å^2/α-helix, respectively.

companion part I under this title (4). The surface pressure rises steeply at an area of ~450 Å^2/α-helix and then reaches a plateau-like region at ~300 Å^2/α-helix. Neither a second steep rise nor an abrupt collapse of the monolayer is observed with decreasing area/helix as the surface pressure steadily increases approaching a minimal area of ~100 Å^2/α-helix.

Bundle orientation and α-helical conformation by x-ray reflectivity

The monolayer electron density profiles obtained from Fresnel-normalized x-ray reflectivity via box refinement (22) are presented in Fig. 3. Analogous to hbAP1 (4), at the lowest surface pressure (π = 30 mN/m) where helices are lying in the plane of air-water interface, the profile exhibits a single maximum at the interface with a width of ~10 Å. This value agrees with the diameter of a single helix's cross-section. The width of this maximum increases steadily extending progressively further into the aqueous subphase as the surface pressure increases. When the monolayer is compressed to 100 Å^2/α-helix (where the surface pressure is ~55 mN/m from the π-A isotherm), the profile is completely uniform extending over ~60 Å along the z axis into the subphase, comparable to the theoretical length of the hbAP-Phe$_{CN}$ α-helix. This result demonstrates, as expected, that the α-helix is the dominant conformation of hbAP-Phe$_{CN}$ protein and all helices orient with their long axis perpendicular to the plane of the interface at an area of 100 Å^2/α-helix.

Coiled-coil four helix bundle structure by GIXD

GIXD data for hbAP-Phe$_{CN}$ (Fig. 4), collected at 100 Å^2/α-helix, exhibit only minor differences from that reported for hbAP1(see Fig. S5 in the Supporting Material for the companion part I under this title) (4). Similarly, a 4-helix bundle with rhombic arrangement in its cross-section provides a better fit to the maximum arising from interhelix interference within the bundle in the background-corrected q_{xy}-dependence of experimental GIXD than a square arrangement. The fitting parameters are ~2.75 Å for helix radius and ~11.25 Å for interhelix separation. The strong primary maximum at $q_z = 0$ Å^{-1} in the q_z-dependence of the interhelix interference maximum, accompanied with the weaker secondary maximum at q_z ~0.20–0.25 Å^{-1} provides the evidence of the coiled-coil conformation, as described by Crick's theory (23,24). Further discussion can be found in the article by Churbanova et al. (5).

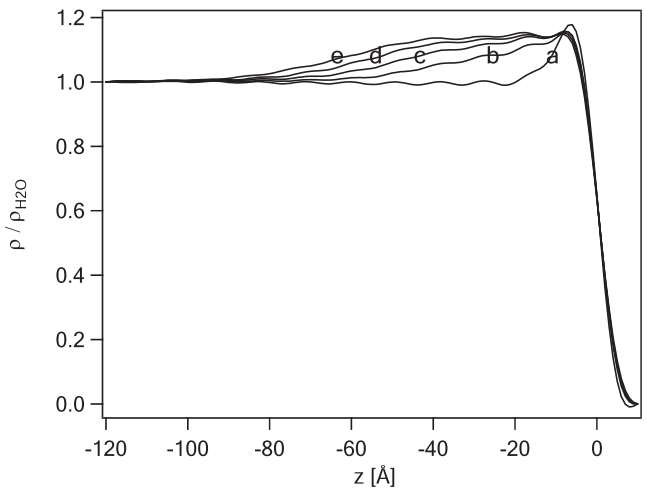

FIGURE 3 Electron density profiles for the hbAP-Phe$_{CN}$ monolayer at various surface pressures or areas. The profile structures were obtained by using the box-refinement algorithm. Profiles labeled from *a* to *e* correspond to the letters in Fig. 2. At π = 30 mN/m, the profile exhibits a single maximum of ~10 Å. At A = 200−150 Å^2/α-helix, the electron density profiles extend more deeply into the subphase with a very broad protein/subphase interface. At A = 120−100 Å^2/α-helix, the profiles show a broad plateau over ~40−60 Å.

Characterizations in isotropic detergent buffer

Secondary structure by CD spectroscopy

The CD spectrum of hbAP-Phe$_{CN}$ (Fig. 5) is measured in an isotropic aqueous detergent solution. The spectrum of hbAP-Phe$_{CN}$ in methanol is also presented as a control. The spectra in both solvents are consistent, displaying two minima at 208 nm and 222 nm, respectively, characteristic of an α-helical conformation. The fractions of α-helical content are ~82% in aqueous buffered detergent solution and 91% in methanol, calculated from Eqs. 1 and 2. The subtle difference in the α-helical content measured in these two solvents is observed for all hbAPn model membrane proteins, where a higher fraction of α-helix is consistently obtained from the protein dissolved in methanol compared to aqueous detergent solution (see Fig. 2 in Ye et al. (3) and Fig. S2 in the companion part I (4)). The results from CD confirm the conclusion drawn from x-ray reflectivity, that the mutations do not significantly alter the secondary structure of the protein, namely it retains a highly α-helical conformation.

Halothane binding affinity by steady-state fluorescence

The fluorescence excitation and emission spectra of hbAP-Phe$_{CN}$ indicate that Phe$_{CN}$ fluorescence is maintained in this model membrane protein (Fig. 6 *A*). The excitation and emission maxima are at 240 nm and 293 nm, respectively, the same as published (13).

The interaction of halothane with the hbAP-Phe$_{CN}$ 4-helix bundle was monitored by intrinsic Phe$_{CN}$ fluorescence quenching, provided in Fig. 6 *B*. Phe$_{CN}$ fluorescence decreases steadily with increasing halothane concentration, as shown in Fig. 6 *C*. Fitting these data to Eq. 3 yields values for the dissociation constant, $K_d = 2.30 \pm 0.05$ mM, and the maximal quenching, $Q_{max} = 1.10 \pm 0.01$. These values are comparable to those of hbAP1, namely a $K_d = 2.5 \pm 0.2$ mM and a $Q_{max} = 1.12 \pm 0.02$ (4), measured under analogous conditions.

The Phe$_{CN}$ fluorescence quantum yield is very sensitive to the local environment of the fluorophore, that is, fluorescence increases by ~10-fold when the solvent is exchanged from

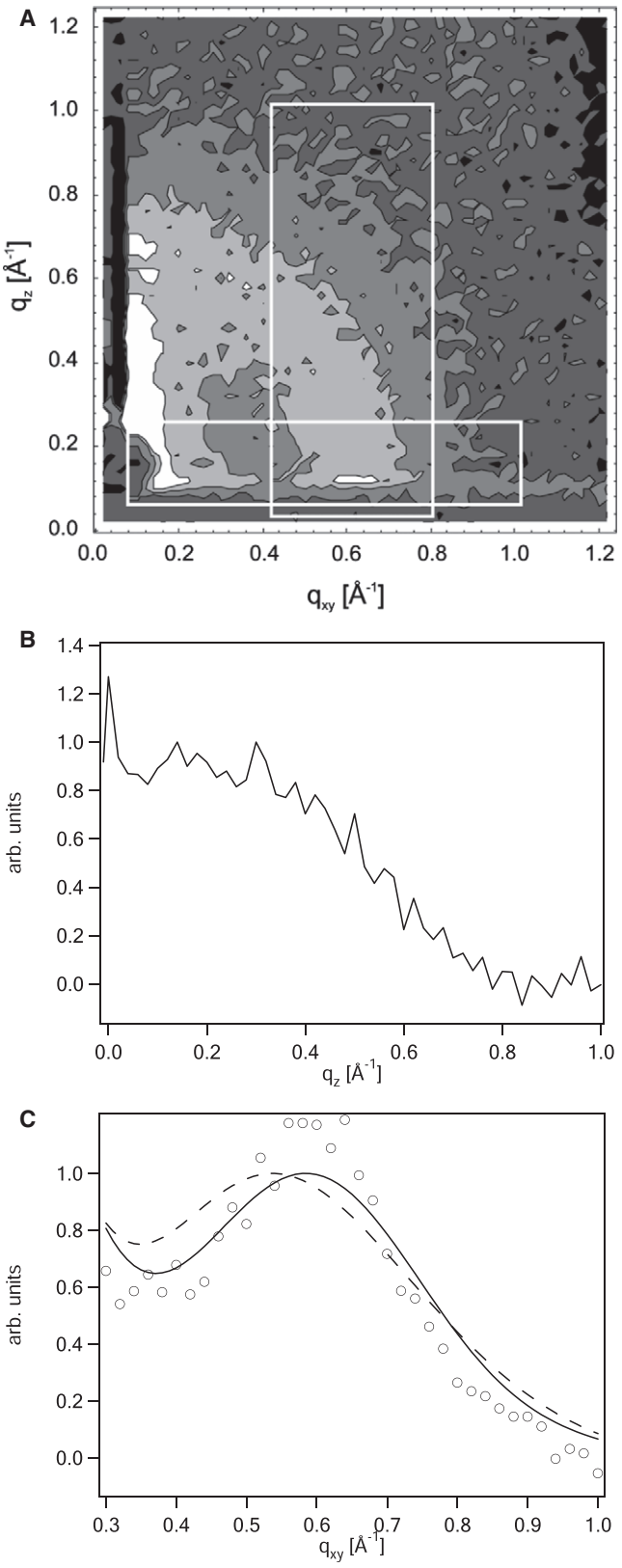

FIGURE 4 GIXD from a Langmuir monolayer of hbAP-Phe$_{CN}$ at 100 Å^2/α-helix. (*A*) Contour plot of experimental GIXD data from hbAP-Phe$_{CN}$ after background correction. The rectangles indicate the region integrated to generate the q_z- and q_{xy}-dependence components. (*B*) The q_z-dependence of the data in *A* integrated over the region indicated by the vertical rectangle. (*C*) The q_{xy}-dependence of the data in *A* integrated over the region indicated by the horizontal rectangle (*circle*), comparing with two model calculations (*dashed* and *solid lines*). The curves are the theoretical q_{xy}-dependence components of the GIXD calculated based on a four-cylinder bundle in a 60° rhombic (*solid curve*) arrangement or a square (*dashed curve*) arrangement in the plane perpendicular to the bundle axis. The experimental Δq_{xy}-resolution = 0.025 Å^{-1} is considered. The radius of each cylinder is 2.75 Å with a nearest-neighbor separation of 11.25 Å for both arrangements.

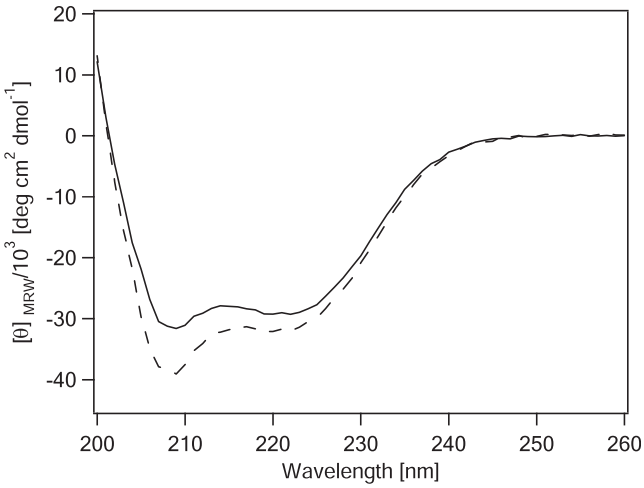

FIGURE 5 CD spectra of hbAP-Phe$_{CN}$ in 50 mM KPi and 500 mM KCl buffer with 0.9% OG at pH 8.0 (*solid line*) and in methanol (*dashed line*). The minima at 208 and 222 nm indicate that hbAP-Phe$_{CN}$ adopts α-helical conformation in both solvents. The fraction of α-helical content is 82% in detergent solution and 91% in methanol, obtained from the mean molar residue ellipticity at 222 nm.

acetonitrile to water (25). The fact that the introduction of halothane into the bundle results only in steadily decreasing fluorescence with increasing halothane concentration suggests that halothane does not promote the dissociation of 4-helix bundles. Any bundle dissociation should lead to a substantial increase in Phe$_{CN}$ fluorescence due to its resulting increased water exposure. Unlike Trp fluorescence, there is no dependence of the wavelength of the emission maximum on solvent polarity for the Phe$_{CN}$ fluorophore.

Comparison of the K_d value of hbAP-Phe$_{CN}$ with that of hbAP1 and hbAP0 shows that the binding affinity for halothane remains virtually the same for all three halothane-binding, amphiphilic 4-helix bundle proteins, implying a successful Trp-to-Phe$_{CN}$ substitution. However, the Met-to-Leu substitution does not significantly improve halothane binding affinity, as observed for the water soluble counterparts (21). This may result from the very different topology for these two types of proteins. The dihelices of the hbAPn model membrane proteins associate with a *syn*-topology, as opposed to the soluble 4-helix bundle proteins, whose dihelices associate with an antitopology. Thus, given the location of the Met residues, they may play a more important role in the soluble proteins by favoring halothane access to bundles,

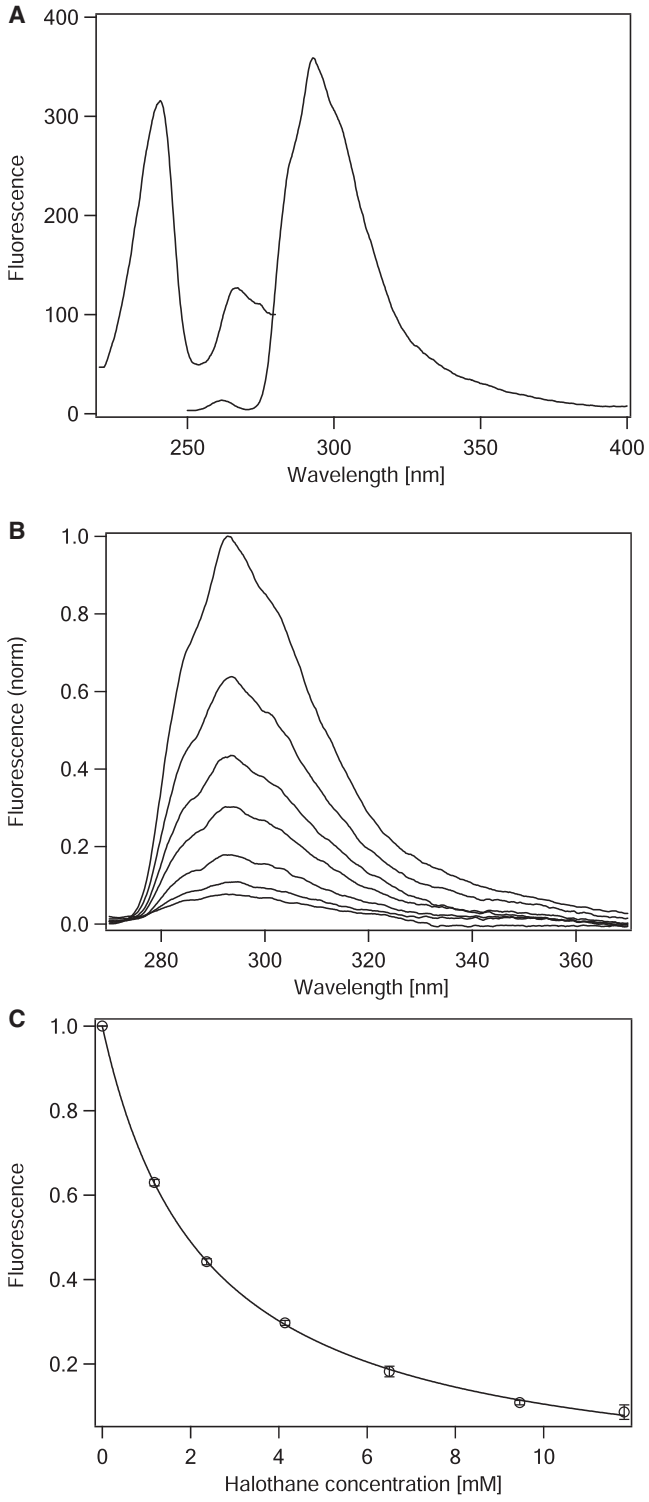

FIGURE 6 (*A*) Fluorescence excitation and emission spectra of 2 μM hbAP-Phe$_{CN}$ in 0.9% OG, 50 mM KPi, and 500 mM KCl (pH 8.0). (*B*) Quenching of hbAP-Phe$_{CN}$ fluorescence as a function of halothane concentration. Excitation was at 240 nm and the emission maximum is at 293 nm. The halothane concentrations were 0, 1.18, 2.37, 4.14, 6.50, 9.46, and 11.83 mM in order of decreasing fluorescence. (*C*) The quenching profile for hbAP-Phe$_{CN}$ by halothane. Data points are the mean of three measurements on separate samples. Error bars represent the standard deviation. The line through the data points is the best fit to Eq. 3, which yields $K_d = 2.30 \pm 0.05$ mM and $Q_{max} = 1.10 \pm 0.01$.

whereas they have no significant effect on amphiphilic 4-helix bundle proteins.

The characterizations described thus far in Results and Discussion indicate that the essential characteristics of the anesthetic-binding, amphiphilic 4-helix bundle proteins, namely the α-helical conformation, the 4-helix bundle structure and halothane binding affinity, are well maintained under this Trp-to-Phe$_{CN}$ mutation. These justify the further investigations of halothane action on the hbAP-Phe$_{CN}$ peptide described below.

Mechanism of fluorescence quenching by fluorescence lifetime

To get a more comprehensive understanding of the mechanism of halothane quenching, fluorescence lifetimes were determined for hbAP-Phe$_{CN}$ in buffered detergent solution at various halothane concentrations (Fig. 7 *A*, *solid triangles*). Phe$_{CN}$ fluorescence lifetimes were obtained by a nonlinear least-squares fitting of the hbAP-Phe$_{CN}$ fluorescence decay profile to three exponentials. A global chi-squared <1.2 as well as randomly distributed residuals served as the goodness-of-fit criteria. Three lifetimes of 8.5 ± 0.1, 1.1 ± 0.1, and 0.14 ± 0.03 ns with corresponding preexponential factors of 7:2:3 were thereby found to be required for the apo form of hbAP-Phe$_{CN}$. The Phe$_{CN}$ amino acid was also studied in H_2O, which yielded a single exponential decay with a lifetime of 7.3 ± 0.1 ns. We therefore assigned the predominant, longest lifetime component for hbAP-Phe$_{CN}$ to Phe$_{CN}$. The reduced τ_0/τ values for this component increase linearly from 1 to ~1.5 with increasing halothane concentration from 0 through ~3 mM, and then remain nearly constant with further elevation in concentration. The reciprocal of the amplitude of hbAP-Phe$_{CN}$ fluorescence emission as a function of increasing halothane concentration is also presented in Fig. 7 *A* (*solid circle*) as a comparison. The reduced fluorescence amplitude data F_0/F curve upward over the entire concentration range, with a slope steeper than that of the lifetime data. At halothane concentrations <3 mM, τ_0/τ is comparable to F_0/F, and for increasing concentrations >3 mM, F_0/F becomes steadily greater than τ_0/τ.

Considering that the affinity for halothane binding to the designed cavity within the hbAP-Phe$_{CN}$ amphiphilic 4-helix bundle is only less than an order of magnitude higher than the affinity for halothane partitioning into nonpolar (''oily'') phase, it is conceivable that there is no exclusive binding site within the nonpolar core of the bundle. In this case, the halothane might be expected to diffuse freely within the core of the bundle, especially at low occupancy. At the same time, owing to the limited volume, the halothane translation would be effectively only one-dimensional. According to the MD simulation, the cross-section of core of hbAP-Phe$_{CN}$ bundle is rhombic with a short diagonal of 7–9 Å (the center to center distance of the β-carbons). The diameter of halothane is ~7 Å, assuming the molecule is spherical. Thus, the nonpolar core is not large enough to accommodate two halothane molecules

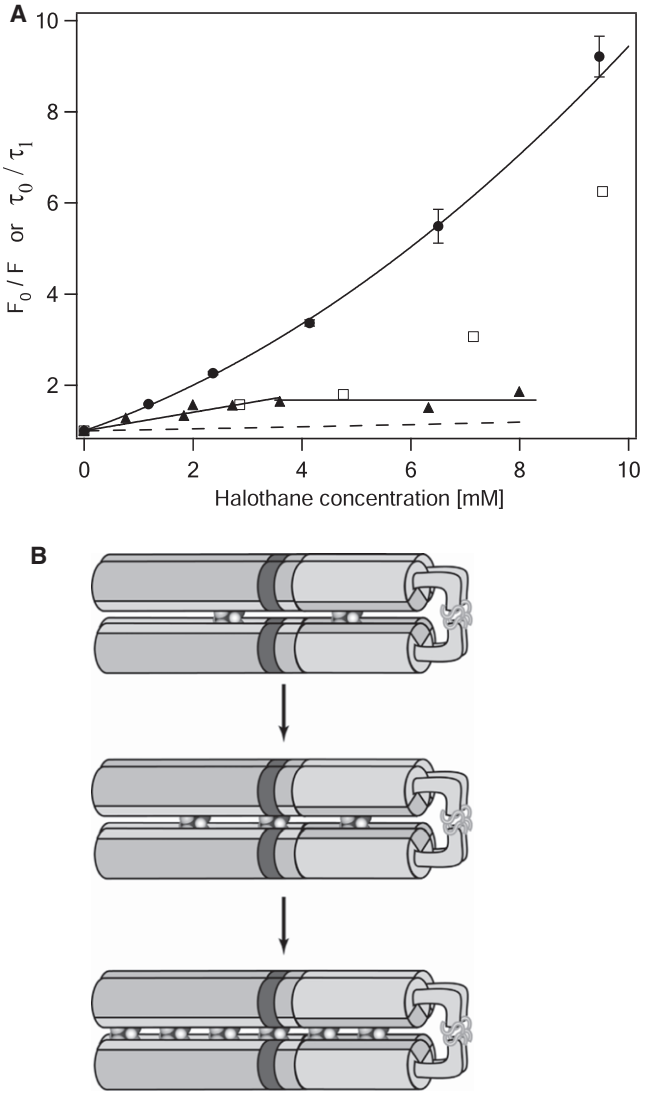

FIGURE 7 (*A*) Stern-Volmer plots for the quenching of hbAP-Phe_{CN} fluorescence, obtained by plotting F_0/F (*solid circle* and *open square*) and τ_0/τ (*solid triangle*) as a function of increasing halothane concentration. The solid line through data points is the best fit. Solid circles represent data collected from hbAP-Phe_{CN} in 0.9% OG, 50 mM KPi, and 500 mM KCl (pH 8.0). Data are the mean of three separate measurements with error bars representing the standard deviation. Open squares stand for data recorded from hbAP-Phe_{CN} multilayer films deposited on an alkylated quartz substrate. Solid triangles are the lifetime results that were collected from measurements on two hbAP-Phe_{CN} solution specimens prepared independently. The dashed line simulates the Stern-Volmer plot of hbAP-Phe_{CN} fluorescence quenching assuming protein bundles dissociate to di-α-helices. (*B*) Illustration of halothane diffusion in hbAP-Phe_{CN} 4-helix bundle as concentration increases. The cylinders represent the α-helices, which are jointed by disulfide bonds formed between the C-terminal Cys residues. The dark gray and light gray halves of each cylinder donate hydrophilic and hydrophobic domains, respectively. The designed binding site Ala^{19} is indicated by the black stripe. Halothane is displayed as a CPK model in the core of the bundle.

side by side. Such one-dimensional diffusion is consistent with x-ray reflectivity results obtained by the investigation of halothane dissociation from the parent hbAP1. Basically, when ~6–7 halothane molecules are confined within one bundle at the maximal halothane concentration, they are uniformly distributed over the length of the bundle. This number of molecules corresponds to approximately one halothane per heptad, which occupies ~10.5 Å along the bundle long-axis. When the concentration is reduced to ~3 halothane per bundle, halothane is then observed to be localized in a broad unimodal distribution centered about the designed cavity with a width of ~27 Å (4). The Phe_{CN} fluorescence emission amplitude and lifetime data described above provide further support of this view. The dependence of fluorescence lifetime on halothane concentration suggests that halothane diffuses one-dimensionally along the core of the protein bundle (Fig. 7 *B*), where a normal diffusion mode is realized at low halothane occupancies of 1–3 per bundle (26). This results in a dynamic quenching mechanism at lower halothane concentrations. At higher occupancy, a single-file diffusion mode is observed (26). The ''blocking effect'' associated with this mode at higher halothane occupancy, the effective confinement of the mean-square displacement of a halothane molecule along the bundle axis due to the presence of first and second nearest neighbor halothane molecules along the core, results in a static quenching mechanism. In particular, at an occupancy of one halothane per heptad, a relatively stable ''dark complex'' would be expected, formed between the halothane molecule in the cavity and the Phe_{CN} residues adjacent the cavity, with essentially no diffusion along the core of the bundle possible.

Characterizations of LB multilayer films on solid substrates

Because of the low solubility of the amphiphilic hbAP-Phe_{CN} even with the presence of detergent coupled with limited sensitivity of the instrument, LB multilayer films were necessarily utilized to detect the infrared absorption due to the nitrile group stretching vibration. Before investigating the effect of halothane binding on this stretching vibration with ATR-FTIR, we characterized the multilayer films primarily to establish whether the 4-helix bundle structure was retained in the films.

Thickness of LB films by x-ray reflectivity

The uniformity and thickness of hbAP-Phe_{CN} films can be obtained from x-ray reflectivity. As seen in Fig. 8 *A* , the Fresnel-normalized reflectivity displays three symmetric maxima of decreasing amplitude with increasing photon momentum transfer q_z and evenly spaced by ~0.07 $Å^{-1}$, indicative of a uniform film of ~90 Å thickness. This thickness can also be derived from the inverse Fourier transform of these data, the Patterson function P(z), which is the autocorrelation function of the gradient electron density profile of the multilayer film (27). The strong maximum in the autocorrelation function at ~90 Å provides a direct measure of this thickness (Fig. 8 *B*). This value is ~1.5 times of the maximum length

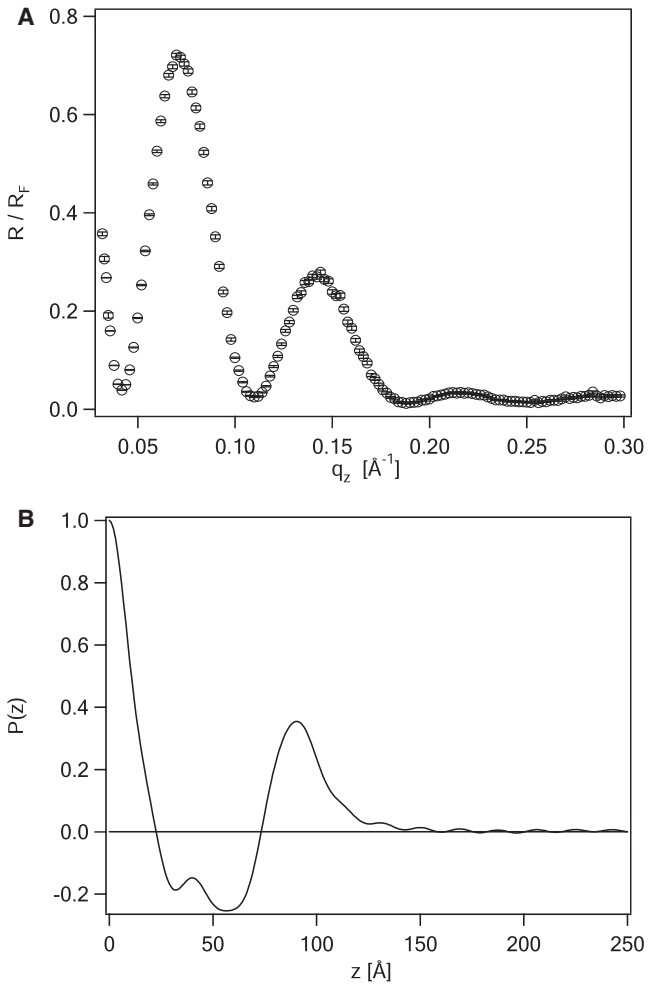

FIGURE 8 (*A*) Fresnel-normalized x-ray reflectivity recorded from hbAP-Phe_{CN} multilayer films deposited on the quartz substrate. The reflectivity profile displays three symmetric maxima of decreasing amplitude with increasing q_z and evenly separated by ~0.07 $Å^{-1}$. (*B*) The Patterson function of the multilayer film calculated from the inverse Fourier transform of data in *A*. The data shows a minimum with a shoulder at ~60 Å and a strong maximum at ~90 Å.

of hbAP-Phe_{CN} helix. It is thereby evident that more than one layer of protein has been deposited on the substrate. Unfortunately, the electron density of hbAP-Phe_{CN} is uniform along the length of the bundle (Fig. 3), and therefore multiple layers, with the long-axis of the bundle either parallel or tilted with respect to the normal to the plane of the quartz substrate within each layer, would be expected to present only a thicker featureless layer in an x-ray reflectivity experiment. However, the actual number of layers can be determined independently (below) from the average tilt-angle derived from dichroic ratio of amide I infrared band in multilayers films on Ge substrates LB-deposited simultaneously with those on quartz.

Halothane binding by steady-state fluorescence

The halothane-induced quenching of fluorescence from hbAP-Phe_{CN} in the form of multilayer films on quartz substrates was characterized (Fig. 9) to verify the preservation of 4-helix bundles during the LB-deposition process. The emission spectrum from hbAP-Phe_{CN} multilayer films appears the same as that for the protein in detergent buffer. The Stern-Volmer plot (F_0/F) describing fluorescence quenching for an hbAP-Phe_{CN} multilayer film (represented by *open squares* in Fig. 7 *A*) exhibits the same upward curvature but with shallower slope. This confirms that halothane is binding to the designed cavity inside the 4-helix bundle of the hbAP-Phe_{CN} protein. If hbAP-Phe_{CN} were to occur in the form of dihelices on the substrate, halothane would be expected to bind to the protein with far less effective quenching, as demonstrated experimentally with the water-soluble, 4-helix bundle model protein counterparts (6) (Fig. 7 *A*, *dashed line*). However, the shallower slope is likely an indication of a more pronounced role for diffusion in the quenching mechanism. As discussed above, the effective dissociation constant for halothane partitioning into a nonpolar (''oily'') phase is only somewhat less than an order of magnitude larger than the dissociation constant for halothane binding to the designed cavity. Such an extended nonpolar phase would be expected to be present in such multilayer films of the amphiphilic 4-helix bundle protein comprised of densely packed monolayers of hydrophobic domains; the presence of such nonpolar phases within the multilayer film would thereby increase the average K_d for apparent halothane binding.

Because the Langmuir monolayer precursor to the LB multilayer films was demonstrated to be comprised of 4-helix bundles of hbAP-Phe_{CN} and the character of halothane binding to protein is maintained for multilayer films LB-deposited onto quartz substrates, it is reasonable to assume that these properties are retained in those multilayer films deposited simultaneously onto Ge substrates from the same precursor monolayer.

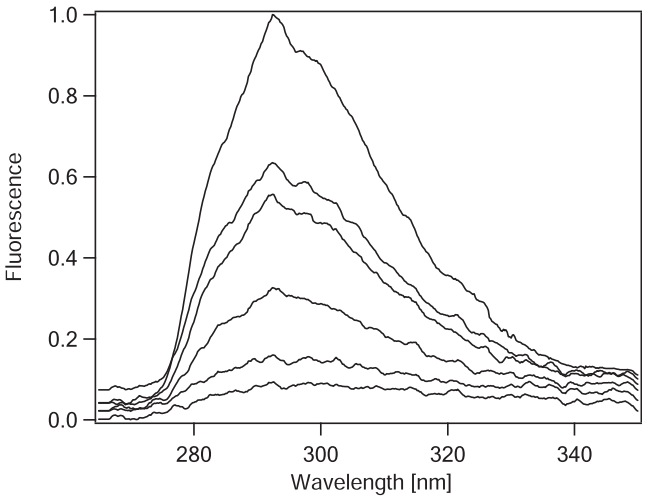

FIGURE 9 Quenching of fluorescence from hbAP-Phe_{CN} in form of multilayer films on quartz substrate as a function of halothane concentration. Excitation was at 240 nm and emission maximum is at 293 nm. The halothane concentrations were 0, 2.9, 4.8, 7.2, 9.5, and 14.3 mM from top to bottom.

Halothane-hbAP-Phe$_{CN}$ interaction by infrared spectroscopy

From Fig. 10 *A*, the symmetric Lorentzian shape of the infrared absorption maximum around ~1654 cm^{-1} with a full width at half-maximum (FWHM) of 23 cm^{-1} can be assigned to the amide I vibrational mode characteristic of a predominant α-helical conformation. The linear dichroism of this vibrational band can be used to reliably calculate the average tilt-angle of the helices with respect to the substrate surface normal. This tilt-angle was thereby determined to be relatively large, namely ~60° under all three halothane conditions spanning the range of halothane concentrations used in the fluorescence quenching experiments. Given this average tilt-angle and the multilayer film thickness of ~90 Å determined by x-ray reflectivity, there are most likely only three layers of the protein LB-deposited on the substrate. This result is not surprising, noting that the interlayer forces effective in the LB-deposition are much weaker for an amphiphilic protein than those for other more typical amphiphiles (e.g., fatty-acids and phospholipids). It is therefore routinely much more difficult to deposit a large number of layers of an amphiphilic protein by LB-deposition. Fig. 10 shows both the amide I band (*A*) and the -CN stretching band (*B*) before exposure to halothane, after exposure to maximal halothane, and after the purge of halothane. Incorporation of halothane into the multilayer of hbAP-Phe$_{CN}$ 4-helix bundle protein induced no change in the amide I band, in terms of either band shape, peak position or dichroic ratio, indicating that the α-helical bundle structure is stable to halothane incorporation.

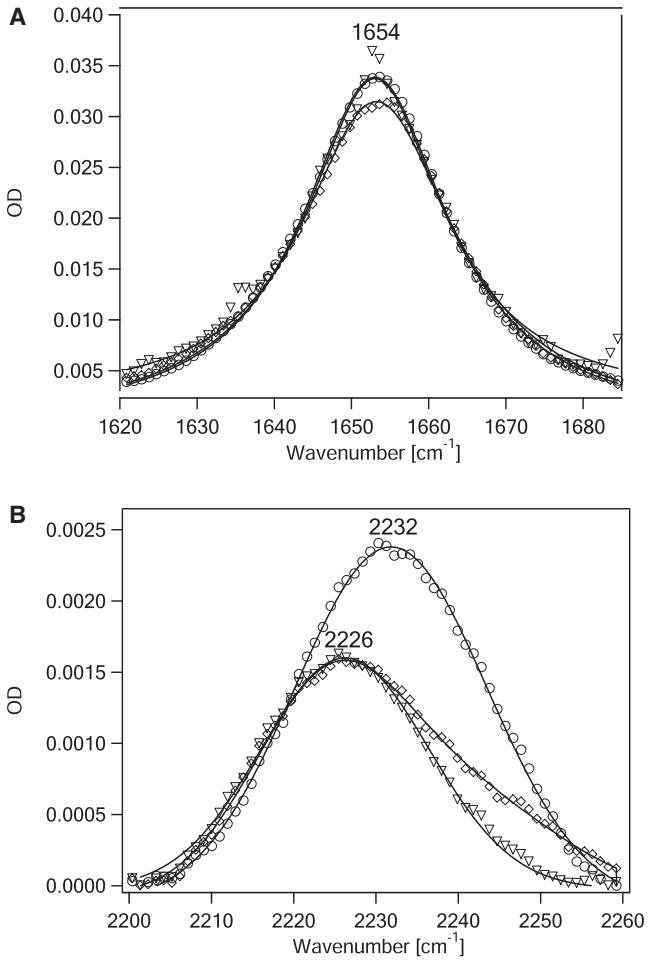

FIGURE 10 Parallel polarization component of the amide I band (*A*) and the -CN stretching vibration band (*B*) of hbAP-Phe$_{CN}$ in the form of multilayer films on a Ge substrate. The triangle, circle, and diamond symbols correspond to spectra collected before exposure to halothane, after exposure to maximal halothane, and after the purge of halothane in both panels. Lines through data points are the best fits using either Loentzian (*A*) or Gaussian (*B*) function. In panel *A*, the best-fit lines for data collected before exposure to halothane and after exposure to maximal halothane are almost superimposed, whereas the one fitting to data obtained after the purge of halothane is slightly lower in intensity. The numbers in this figure indicate the positions of maxima.

Given the above with regard to the amide I band, we note that the signal from the -CN stretching vibration is more than an order of magnitude weaker and is not readily observable before background subtraction. Furthermore its width suggested that it might be difficult to measure any relatively small shifts in its peak position as a function of halothane incorporation into the hbAP-Phe$_{CN}$ bundle. We therefore chose to investigate the effect of halothane on this vibration only at a maximal halothane concentration (~14.3 mM) sufficient to fully quench fluorescence emission to obtain a reproducible result. Fig. 10 *B* shows the parallel polarization component of -CN stretching vibration band. Unlike the amide I band, a Gaussian function is required to provide the best fit for -CN stretching band under all three conditions. The FWHM of -CN band is 24 cm^{-1} before halothane exposure and 27 cm^{-1} with the presence of halothane. The broad Gaussian band shape reveals the inhomogeneity of the four -CN probes within one bundle, caused by their nonequivalent local environments. The broad Gaussian band shape can be well fit with two pairs of Lorentzians, each with a FWHM of ~10 cm^{-1} for the pair at lower wavenumbers and ~14 cm^{-1} for the pair at higher wavenumbers, and a maximal separation of the centers of the four Lorentzians of 10 cm^{-1}. These values are comparable to those previously reported, namely the FWHM of the stretching band for a single -CN in a polypeptide (10) and the difference between the centers of -CN bands in polar versus nonpolar solvents (9). The inhomogeneity of the probes has been justified by MD simulation, provided in Table 2 in part III under this title. The four -CN oscillators are found to occur as two pairs within the 4-helix bundle based on the water accessibility, namely, two of them are buried in the nonpolar interior of the bundle, whereas the other pair is oriented more toward the exterior, partially accessible to water. Moreover, each member of the pair also experiences a slightly different local environment. These nonequivalent local environments predict the centers of the -CN bands to be maximally separated by ~8–12 cm^{-1} (28). The center of the -CN band shifts from ~2226 cm^{-1} before halothane exposure to ~2232 cm^{-1} after exposure to maximal halothane, and

then back to ~2226 cm^{-1} after a purge of halothane. The band position before halothane exposure is close to that of Fmoc-Phe_{CN} in tetrahydrofuran (9), indicating that the -CN groups are mostly buried inside the nonpolar core of the bundle. After equilibration with maximal halothane, the center of -CN band shifts to a higher frequency by almost 6 cm^{-1}. The small magnitude of this blue-shift implies that the -CN groups remain in a generally hydrophobic environment. A similar blue-shift is observed for the Phe_{CN}-labeled mastoparan x dissolved in sodium bis-(2-ethylhexyl) sulfosuccinate reverse micelles (11). In that work, the blue-shift is larger and was attributed to a hydrogen bond between the -CN group and a water molecule. This might suggest the possibility of a similar H-bond formation between the -CN group and halothane hydrogen. However MD simulations reveal that the origin of the observed blue-shift is more likely a halothane-induced change of electrostatic protein environment of the -CN groups, as described in the companion part III under this title (28). After the halothane purge, the -CN band shifts back to its original position (~2226 cm^{-1}) but the band-width is still slightly broader. This somewhat less than full reversibility is consistent with that observed in both the fluorescence quenching (5) and x-ray reflectivity (4) experiments. Finally, we note that the perpendicular polarization component of this -CN stretching band is too weak to be reliably determined after background subtraction. We also mention here that we did investigate a thicker film prepared by simply spreading hbAP-Phe_{CN} from methanol solution onto a Ge substrate, followed by rehydration under moist nitrogen. Although this film was not similarly characterized as for the LB-deposited multilayer films, nevertheless an entirely similar reversible blue-shift of comparable magnitude was observed upon exposure to halothane under otherwise identical conditions (data not shown).

It is particularly important to note here that the infrared absorption arising from this -CN stretching vibration arises from the superposition of all four -CN groups in the 4-helix bundle (i.e., at one group per helix). As mentioned above, all-atom MD simulations in explicit solvent suggest that these four groups are not equivalent, each group experiencing a slightly different local environment. These nonidentical local environments provide the origin of the broad Gaussian band shape and possibly the asymmetry of the band shape as well. Thus, the four nonidentical probes increase the complexity of the system, and in addition, the fluorescence quenching mechanism has been shown in this work to be dynamic for a small number of halothane molecules per bundle. As a result, MD simulation appears to be essential to provide a quantitative interpretation of the infrared results reported here. The results from such simulations are reported in companion part III under this title (28).

CONCLUSIONS

This study demonstrates that Phe_{CN} is a successful substitution for Trp in the investigation into the nature of the interaction of the inhalational anesthetic halothane with a model membrane protein. This mutation offers a more definitive physical probe of the halothane binding mechanism without altering physical-chemical characteristics of the halothane-binding model membrane protein. Fluorescence lifetime analysis for hbAP-Phe_{CN} as a function of halothane concentration reveals that halothane diffuses one-dimensionally along the core of the amphiphilic 4-helix bundle protein, which results in dynamic quenching at lower concentrations and static quenching at higher concentrations. This result is consistent with x-ray reflectivity measurements on the interaction of halothane with hbAP1, the parent protein in the same family of halothane-binding, amphiphilic 4-helix bundle model membrane proteins. The infrared results demonstrate a reversible blue-shift of the -CN stretching vibrational band in the presence of halothane. The complexity of this system requires an interpretation via MD simulations. These simulations show that the frequency shift is more likely due to a change in the electrostatic protein environment of the -CN groups induced by halothane, rather than a direct hydrogen-bonding interaction with halothane. With a stronger polarized infrared light source as provided by synchrotron radiation and a more sensitive detector, we should be able to determine the averaged orientation of -CN groups within single monolayer specimens, information that would further contribute to better understanding the binding mechanism. Furthermore, the -CN group can also be used to label Ala, the residues forming the binding cavity. The nitrile-derivatized Ala could provide even more direct information about the nature of inhalational anesthetics binding to this model membrane protein.

The authors thank Thomas Troxler for assistance and helpful discussion on the fluorescence lifetime acquisition and data analysis at the Regional Laser and Biomedical Technology Laboratories supported by National Institutes of Health grant P41RR001348; Feng Gai for supply of the CD spectropolarimeter and infrared spectrometer; Paul Heiney for providing the triple-axis diffractometer facility, supported by the Materials Research Science and Engineering Center program of the National Science Foundation (grant No. DMR05-20020); Venkaka Krishnan for assistance with x-ray data collection; Mike Sullivan for use of the support lab at the Case Center for Synchrotron Biosciences; Benjamin M. Ocko, Elaine Dimasi, and Scott Coburn for technical assistance at beamline X22-B at the National Synchrotron Light Source, Brookhaven National Laboratory; and Ivan Kuzmenko and Thomas Gog for technical assistance at Sector 9 at the Advanced Photon Source, Argonne National Laboratory.

The synchrotron light sources at National Synchrotron Light Source and Advanced Photon Source are supported by the U.S. Department of Energy, Office of Science, Office of Basic Energy Sciences, under contract No. DE-AC02-98CH10886 and No. DE-AC02-06CH11357, respectively. This work was supported primarily by the National Institutes of Health grant P01-GM55876.

REFERENCES

1. Eckenhoff, R. G., and J. S. Johansson. 1997. Molecular interactions between inhaled anesthetics and proteins. *Pharmacol. Rev.* 49:343–367.
2. Franks, N. P., and W. R. Lieb. 1994. Molecular and cellular mechanisms of general-anesthesia. *Nature*. 367:607–614.

3. Ye, S. X., J. Strzalka, I. Y. Churbanova, S. Y. Zheng, J. S. Johansson, et al. 2004. A model membrane protein for binding volatile anesthetics. *Biophys. J.* 87:4065–4074.
4. Strzalka, J., J. Liu, A. Tronin, I. Y. Churbanova, J. S. Johansson, et al. 2009. Mechanism of interaction between the general anesthetic halothane and a model ion channel protein, I: structural investigations via x-ray reflectivity from Langmuir monolayers. *Biophys. J.* 96:4164–4175.
5. Churbanova, I. Y., A. Tronin, J. Strzalka, T. Gog, I. Kuzmenko, et al. 2006. Monolayers of a model anesthetic-binding membrane protein: formation, characterization, and halothane-binding affinity. *Biophys. J.* 90:3255–3266.
6. Johansson, J. S., B. R. Gibney, F. Rabanal, K. S. Reddy, and P. L. Dutton. 1998. A designed cavity in the hydrophobic core of a four-alpha-helix bundle improves volatile anesthetic binding affinity. *Biochemistry.* 37:1421–1429.
7. Barth, A., and C. Zscherp. 2002. What vibrations tell us about proteins. *Q. Rev. Biophys.* 35:369–430.
8. Yoshikawa, S., D. H. Okeeffe, and W. S. Caughey. 1985. Investigations of cyanide as an infrared probe of hemeprotein ligand-binding sites. *J. Biol. Chem.* 260:3518–3528.
9. Getahun, Z., C. Y. Huang, T. Wang, B. De Leon, W. F. DeGrado, et al. 2003. Using nitrile-derivatized amino acids as infrared probes of local environment. *J. Am. Chem. Soc.* 125:405–411.
10. Tucker, M. J., Z. Getahun, V. Nanda, W. F. DeGrado, and F. Gai. 2004. A new method for determining the local environment and orientation of individual side chains of membrane-binding peptides. *J. Am. Chem. Soc.* 126:5078–5079.
11. Mukherjee, S., P. Chowdhury, W. F. DeGrado, and F. Gai. 2007. Site-specific hydration status of an amphipathic peptide in AOT reverse micelles. *Langmuir.* 23:11174–11179.
12. Reimers, J. R., and L. E. Hall. 1999. The solvation of acetonitrile. *J. Am. Chem. Soc.* 121:3730–3744.
13. Tucker, M. J., R. Oyola, and F. Gai. 2005. Conformational distribution of a 14-residue peptide in solution: A fluorescence resonance energy transfer study. *J. Phys. Chem. B.* 109:4788–4795.
14. Johansson, J. S., R. G. Eckenhoff, and P. L. Dutton. 1995. Binding of halothane to serum-albumin demonstrated using tryptophan fluorescence. *Anesthesiology.* 83:316–324.
15. Tatulian, S. A., and L. K. Tamm. 2000. Secondary structure, orientation, oligomerization, and lipid interactions of the transmembrane domain of influenza hemagglutinin. *Biochemistry.* 39:496–507.
16. Luo, P. Z., and R. L. Baldwin. 1997. Mechanism of helix induction by trifluoroethanol: A framework for extrapolating the helix-forming properties of peptides from trifluoroethanol/water mixtures back to water. *Biochemistry.* 36:8413–8421.
17. Holtom, G. R. 1990. Artifacts and diagnostics in fast fluorescence measurements. *Proc. SPIE.* 1204:2–12.
18. Vigano, C., L. Manciu, F. Buyse, E. Goormaghtigh, and J. M. Ruysschaert. 2000. Attenuated total reflection IR spectroscopy as a tool to investigate the structure, orientation and tertiary structure changes in peptides and membrane proteins. *Biopolymers.* 55:373–380.
19. Tamm, L. K., and S. A. Tatulian. 1993. Orientation of functional and nonfunctional pts permease signal sequences in lipid bilayers - a polarized attenuated total-reflection infrared study. *Biochemistry.* 32: 7720–7726.
20. Yamamoto, K., and A. Masui. 1995. Complex refractive-index determination of bulk materials from infrared reflection spectra. *Appl. Spectrosc.* 49:639–644.
21. Johansson, J. S., D. Scharf, L. A. Davies, K. S. Reddy, and R. G. Eckenhoff. 2000. A designed four-alpha-helix bundle that binds the volatile general anesthetic halothane with high affinity. *Biophys. J.* 78:982–993.
22. Zheng, S., J. Strzalka, D. H. Jones, S. J. Opella, and J. K. Blasie. 2003. Comparative structural studies of Vpu peptides in phospholipid monolayers by x-ray scattering. *Biophys. J.* 84:2393–2415.
23. Crick, F. H. C. 1953. The packing of alpha-helices - simple coiled-coils. *Acta Crystallogr.* 6:689–697.
24. Crick, F. H. C. 1953. The Fourier transform of a coiled-coil. *Acta Crystallogr.* 6:685–689.
25. Tucker, M. J., R. Oyola, and F. Gai. 2006. A novel fluorescent probe for protein binding and folding studies: p-cyano-phenylalanine. *Biopolymers.* 83:571–576.
26. Borman, V. D., B. Johansson, N. V. Skorodumova, I. V. Tronin, V. N. Tronin, et al. 2006. Diffusion and particle mobility in 1D system. *Phys. Lett. A.* 359:504–508.
27. Blasie, J. K., S. Zheng, and J. Strzalka. 2003. Solution to the phase problem for specular x-ray or neutron reflectivity from thin films on liquid surfaces. *Phys. Rev. B.* 67:224201.
28. Zou, H. L., J. Liu, and J. K. Blasie. 2009. Mechanism of interaction between the general anesthetic halothane and a model ion channel protein, III: molecular dynamics simulation incorporating a cyanophenylalanine spectroscopic probe. *Biophys. J.* 96:4188–4199.